Idaho State University

Natural Buttes Gas Field Land Deformation Detection Using Sentinel-1 InSAR

Christina Appleby

GEOL 6609: Advanced Remote Sensing

Professor Bottenberg

April 9, 2024

Abstract

Fluid extraction from the ground can lead to land subsidence above the extraction area. Since land subsidence is a slow process, detection can be difficult. This study aimed to detect land subsidence as a result of gas extraction in and around the Natural Buttes gas field in northeastern Utah. Sentinel-1 imagery was used to perform DInSAR and SBAS InSAR analysis from June 29, 2017 to July 30, 2018. Both subsidence and uplift were detected in the study area.

1. Introduction

1.1 Interferometric Synthetic Aperture Radar

Synthetic Aperture Radar (SAR) is a type of remote sensing data captured by satellites orbiting the Earth. Unlike multispectral sensors that record light from the sun reflected off the surface, SAR sensor produces its own energy and records the energy that is reflected from the surface. As a result, data collection can occur day or night. The phase and amplitude of the reflected energy is recorded. Synthetic aperture allows SAR imagery to have a high resolution with a shorter antenna, which combines a series of acquisitions that simulate using a larger antenna (Hall, 2023).

The SAR sensors can operate in different wavelength bands. Of the currently active and popular SAR satellites, Sentinel-1 operates in the C-band (7.5 to 3.8 centimeters) and TerraSAR-X operates in the X-band (3.8 to 2.4 centimeters). The wavelength affects how the radar signal interacts with surface, as well as how far it can penetrate. Shorter wavelengths, such as the X-

band, cannot penetrate through foliage, whereas the C-band can only penetrate through the top layers of foliage in a forest canopy (Hall, 2023).

Interferometric Synthetic Aperture Radar (InSAR) can be used to determine the differences in the surface (deformation) by processing two images acquired from the same area at two different times. The phase recorded by the SAR sensor is used to determine the distance between the surface and the sensor, and the differences are captured in an interferogram. When selecting images for InSAR, there are a few conditions that must be met. The two images must be from the same orbit direction, frame, and path, should ideally be from the same sensory or an identical sensor, and have the same polarizations. Another consideration is the baselines. The perpendicular baseline is the physical distance between the position of the two satellites when the image was acquired. The temporal baseline is the amount of time between image acquisitions (Alaska Satellite Facility, n.d.).

Differential InSAR (DInSAR) is one type of InSAR technique, and the workflow can be seen in Figure 1. The phase differences between the two images are used to generate an interferogram, and during interferogram formation, the topographic phase is also subtracted. (Suhadha & Julzarika, 2022). However, changes in the surface are not the only factors that affect phase change; atmospheric delay, topographic effects, and noise can affect the interferogram (Suganthi & Elango, 2020). In addition to the interferogram, the coherence is estimated between the two images, with values ranging from 0 to 1, 0 meaning the pixel is not at all similar between the two images and 1 meaning they are exactly the same. Permanent infrastructure usually has high coherence, and vegetation usually has lower coherence. For deformation monitoring, a small perpendicular baseline and short temporal baseline are desirable to maximize coherence (Suhadha & Julzarika, 2022).

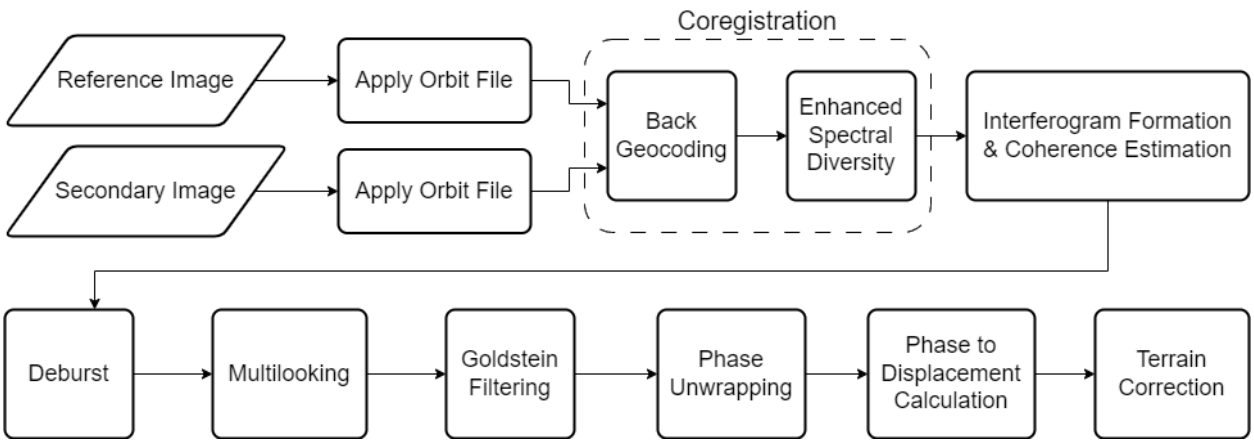

Figure 1 - DInSAR workflow.

The values of generated interferogram are in phase, which are ambiguous. As a result, the interferogram is unwrapped, where the absolute phase value is obtained and converted to meters (Muhammad & Apichontrakul, 2023). The unwrapped interferometric phase is then converted to a displacement map. When the earlier image is used as the reference image, negative values on the displacement indicate subsidence and positive values indicate uplift.

The DInSAR technique utilizes a single interferogram, and as previously mentioned, atmospheric effects and noise can induce error into the interferogram. To minimize these errors, two different techniques of time-series InSAR analysis can be performed, Persistent Scatter InSAR (PSInSAR) and Small Baseline Subset InSAR (SBAS) (Li et al., 2022). Both time series techniques reveal patterns in deformations over time. As the name implies, PSInSAR focuses on persistent or permanent scatters with high phase stability and coherence between images, such as permanent structures. This technique is particularly effective in urban areas. A network of at least 20 interferograms with one reference image are analyzed (Karamvasis & Karathanassi, 2020).

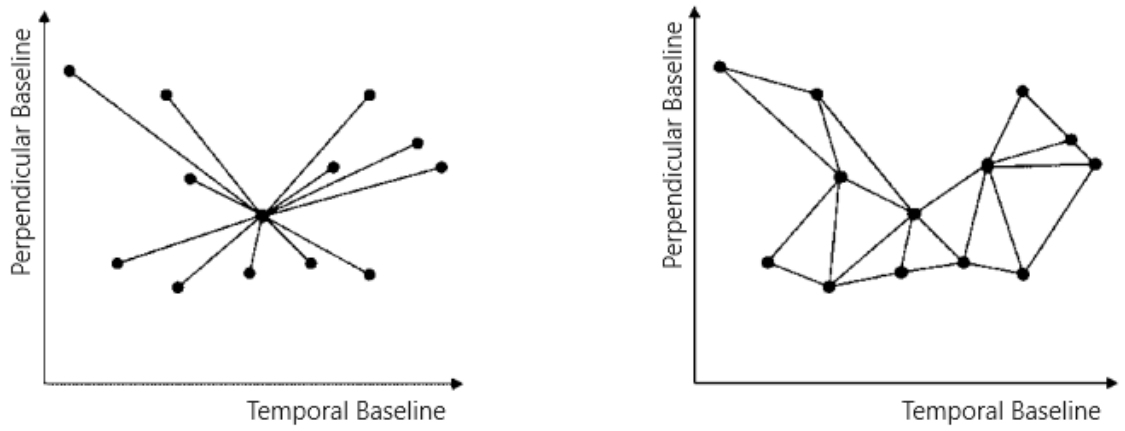

Figure 2 - Example baseline plots for PSInSAR (left) and SBAS (right). Each point is an image, and each connecting line is an interferogram.

The SBAS technique utilizes multilook DInSAR interferograms created from image pairs that form a redundant network. The image pairs used have small perpendicular baselines and moderate temporal baselines, although the temporal baselines are considerably shorter compared to PSInSAR. SBAS analyzes the difference between the image pairs, and because of the short baselines, errors are minimized. This technique is especially useful in areas with lower coherence (Chen et al., 2020).

There are various software options available for InSAR processing. The European Space Agency (ESA) Sentinel Applications Platform (SNAP) is a popular choice for generating interferograms using Sentinel-1 data. An external tool, snaphu is used inside of SNAP to unwrap the interferograms. For PSInSAR, the Stanford Method for Persistent Scatters (StaMPS) is often cited in literature; however, the software package is no longer maintained. Another software package that is frequently cited for PSInSAR is SARproZ, which is actively maintained. For SBAS analysis, the Miami InSAR Time-Series (MintPy) Python is commonly cited.

1.2 Objectives

InSAR has been used in detecting and measuring ground deformations in various cases, such as landslides, earthquakes, land subsidence, and volcanic activity. Land subsidence can be caused by many things, such as fluid extraction and mining. Groundwater extraction is a leading cause in land subsidence; however, oil and gas extraction are known to cause land subsidence as well (Bagheri-Gavkosh et al., 2021). A study performed on the Thace region of Turkey discovered a strong correlation between land subsidence and natural gas extraction rates from 2014 to 2020 (Nozadkhalil et al., 2023).

The objective of this study was to detect subsidence in the vicinity of the Natural Buttes gas field in northeastern Utah, by processing Sentinel-1 imagery using DInSAR and SBAS for comparison. Areas of uplift were expected because of the fracking and gas extraction. The coherence of the SBAS interferograms was expected to be high because of the time series, and there is very little vegetation in the study area. Because of the large temporal baseline of the DInSAR analysis, the coherence was expected to be lower. Lastly, a supervised image classification was performed for the area surrounding Natural Buttes.

1.3 Study Area

The Uinta-Piceance Basin is in the northeastern corner of Utah (Uinta) and spans to the northwestern corner of Colorado (Piceance). The Upper Cretaceous Mesaverde Group is a total petroleum system in the basin that is approximately 20,000 square miles. The Mesaverde Group primarily produces gas and has a maximum depth of about 19,000 feet in the Unita Basin (USGS Uinta-Piceance Assessment, 2003). The Greater Natural Buttes gas field is in the Uinta Basin,

and gas from this field comes primarily from the Mesaverde group. The Natural Buttes gas field is part of Greater Natural Buttes and is the largest gas field in Utah.

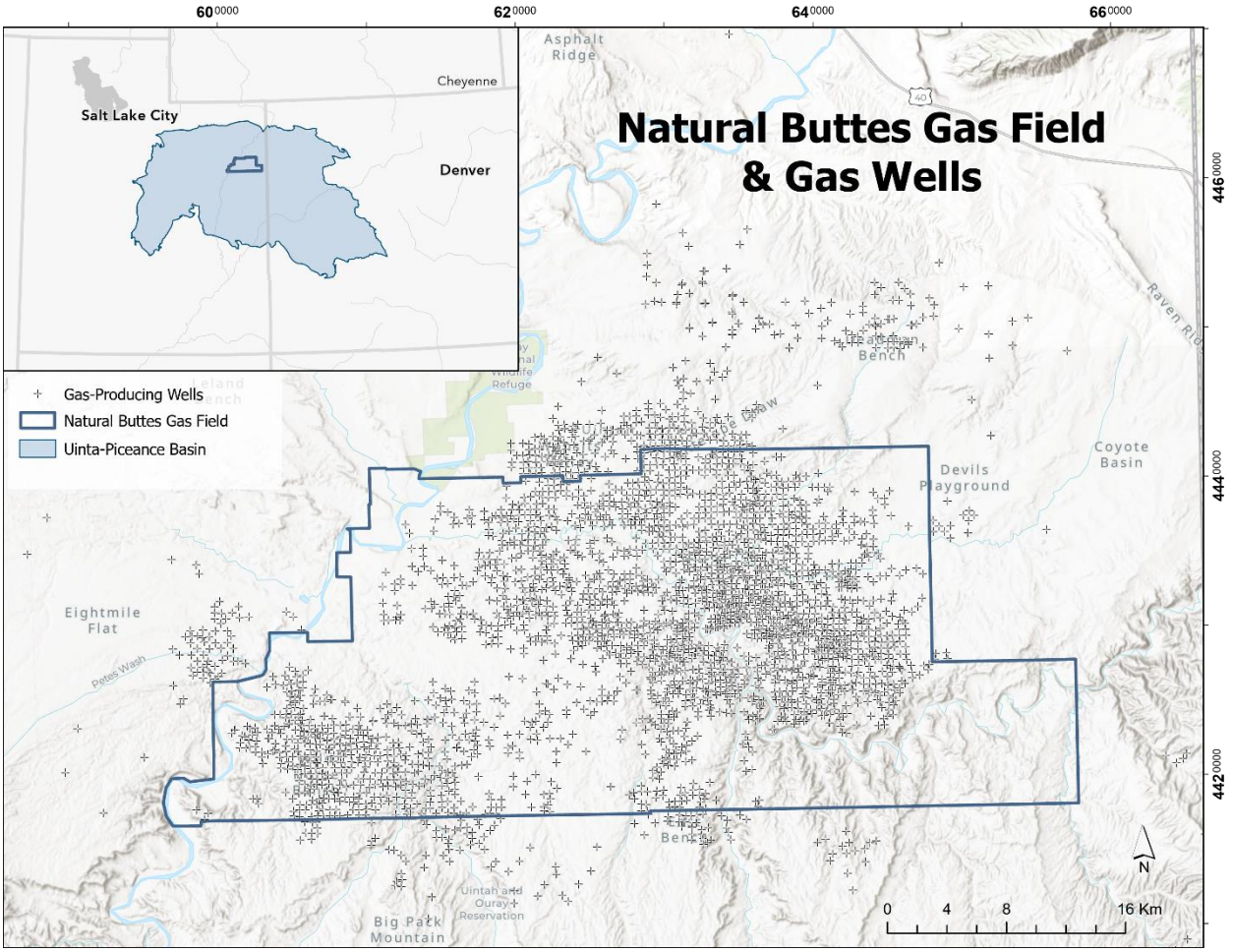

Figure 3 - Natural Buttes gas field is in northeastern Utah.

The tight gas sandstone in the reservoir rock, meaning the permeability of the rock is very low. As a result, wells are closely spaced together in the GNB gas field (Chidsey, 2016), and as of October 2022, the area served over 4,000 gas-producing wells (Chidsey, 2022). Additionally, fracking is necessary to extract the gas. Gross gas withdrawals for only the GNB field could not

be found, but from 2020 to 2022 averaged approximately 170,000 million cubic feet per year (U.S. Energy Information Administration, 2024).

2. Data and Methods

2.1 Data

Sentinel-1A Level 1 Single Look Complex (SLC) interferometric wide swath (IW) imagery was acquired using the ESA Copernicus Browser for descending orbits. The Sentinel-1 satellites carry C-SAR instruments that operate at the C-band wavelength. The temporal resolution of both Sentinel-1A and 1B is 12 days, and the two satellites' orbits are offset by six days. As a result, using imagery from both satellites can decrease temporal resolution to six days. The IW imagery contains three swaths, and within each swath are numerous sub-swaths, or bursts.

For the SBAS analysis, interferograms processed by the Alaska Satellite Facility (ASF) HyP3 service from Sentinel-1 imagery were used. The ASF Data Search Vertex portal has an SBAS feature, which automatically creates image pairs based on the dates, location, and temporal and perpendicular baseline. A temporal baseline of 36 days and a perpendicular baseline of 100 meters were used for the search criteria based on Chen et al. (2020). A total of 34 images were used to create 81 image pairs.

Gas extraction in Utah peaked in 2012 with approximately 403,000 million cubic feet of gas withdrawn, and the volume extracted decreased every year until 2021 where approximately 166,000 million cubic feet of gas was withdrawn (U.S. Energy Information Administration, 2024). Using images closer to 2012 when gas extraction was highest would have been ideal;

however, very few image pairs were available until 2017. Images from June 29, 2017 to July 30, 2018 created enough image pairs for an SBAS analysis, and only images from the descending orbit were selected. The network of image pairs with their spatial coherence can been seen in (Figure 4). Sentinel-1A images for June 29, 2017, and July 30, 2018, were chosen for DInSAR because the summer months are driest and reduce atmospheric errors. Although coherence is generally lower with higher temporal baselines, the two image dates are approximately one year apart since land subsidence is a very slow process.

Sentinel-2A Level 2A multispectral imagery for July 24, 2018 and August 6, 2018 was also acquired using the ESA Copernicus Browser. The imagery is 100 by 100 kilometers, and the spectral resolution of the bands range from 10 meters to 60 meters.

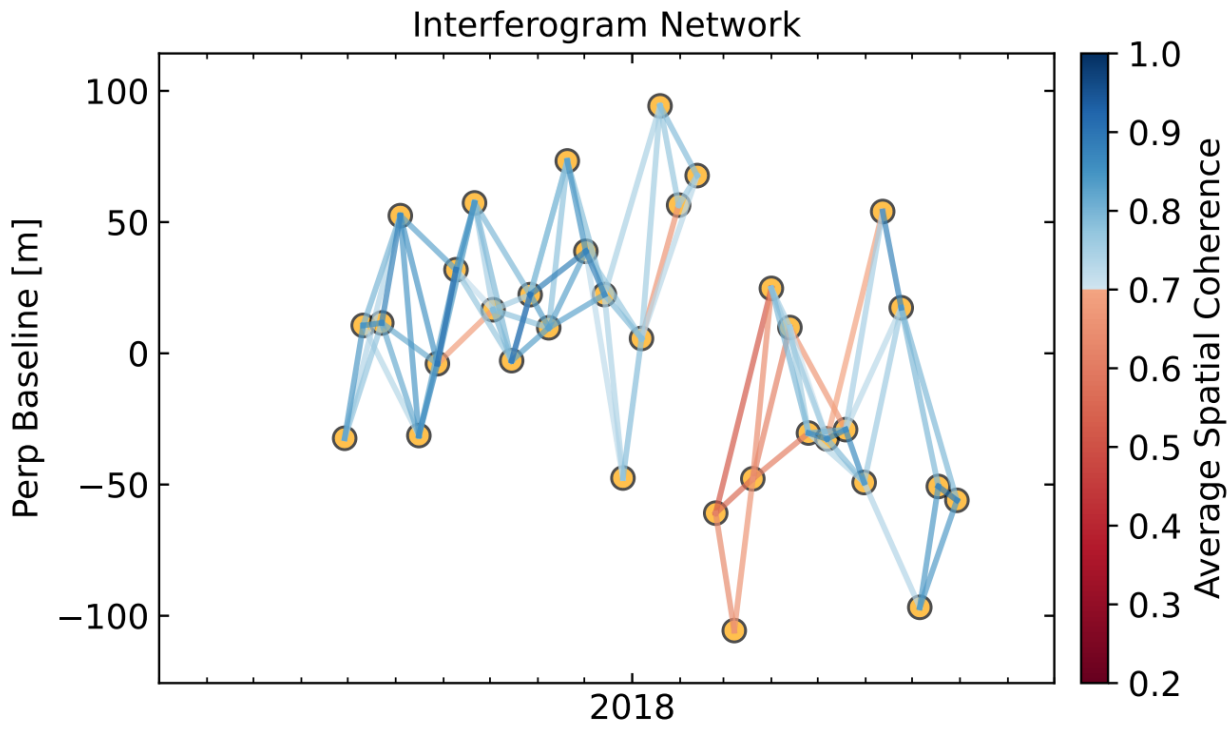

Figure 4 - SBAS interferogram network with average spatial coherence for image pairs from June 29, 2017 to July 30, 2018. Each point is an image date, and the line connecting the points is an image pair.

2.2 Methods

The Sentinel-1A imagery downloaded from the ESA Copernicus Browser were processed using the ESA SNAP software following the DInSAR workflow in Figure 1 with a few additional steps. Sub-swaths 3 through 6 of IW1, IW2, and IW3 were selected for processing using TOPSAR Split prior to applying the orbit files. All three swaths were used because it was unclear which swaths covered the study area. After deburst, the three IW swaths were merged, subset to the study area, and processing continued with one image. The parameters for the multilooking resulted in a pixel size of approximately 18 meters. SRTM 1-Sec HGT was selected as the digital elevation model (DEM) and was automatically downloaded by SNAP for the back geocoding, interferogram formation, and terrain correction.

After image pair selection in the ASF Data Search Vertex portal, the OnDemand interferogram processing was used. For processing options, the number of looks to take in the range in azimuth was set to 10x2, the adaptive phase filter was set to 0.6, and the option to include the DEM and look factors was selected because they are necessary for MintPy processing.

The ASF operates a JupyterHub computing environment called OpenScienceLab and uses data from NASA's Distributed Active Archive Center, which includes Sentinel-1 data. It is free to use and includes ASF's OpenSARLab that is designed specifically for InSAR workflows. In the OpenSARLab, a Jupyter Book containing Notebooks for creating a conda environment with the necessary Python packages, creating an account with the Copernicus Climate Data Store (CDS) to access data for tropospheric corrections, preparing the InSAR image stack for analysis, and performing the SBAS time series analysis using MintPy. All the Notebooks were executed, and the analysis workflow can be seen in Figure 6.

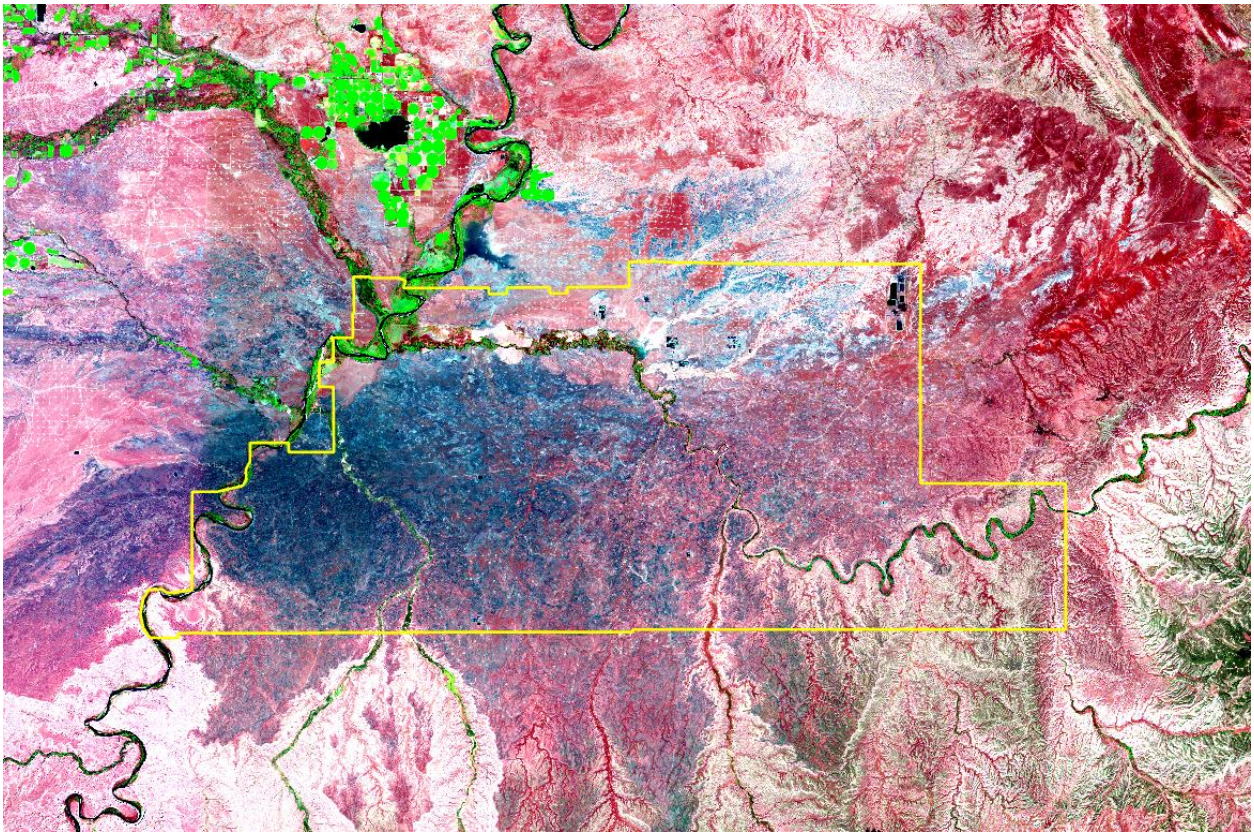

Figure 5 - False color composite of the study area RGB Bands 11, 8, 5.

For the SBAS processing, MintPy determined the reference point, and the earliest date in the image stack was chosen as the reference point. Tropospheric propagation delays were corrected for using European Centre for Medium-Range Weather Forecasts Reanalysis v5 (ECMWF ERA5) pressure data from the CDS. DEM errors were also corrected for.

The Sentinel-2A Bands 2 - 4 and 8 with a spatial resolution of 10 meters and Bands 5 - 7, and 11 and 12 with a spatial resolution of 20 meters were brought in the ENVI software. The bands were stacked, and the 20-meter resolution bands were resampled to 10 meters. The images from the two dates were then mosaicked and subset to the study area. Four regions of interest were selected and used to perform the image classification using the spectral angle mapper algorithm.

Additional regions of interest for the same classes were also selected to produce a confusion matrix for the accuracy assessment.

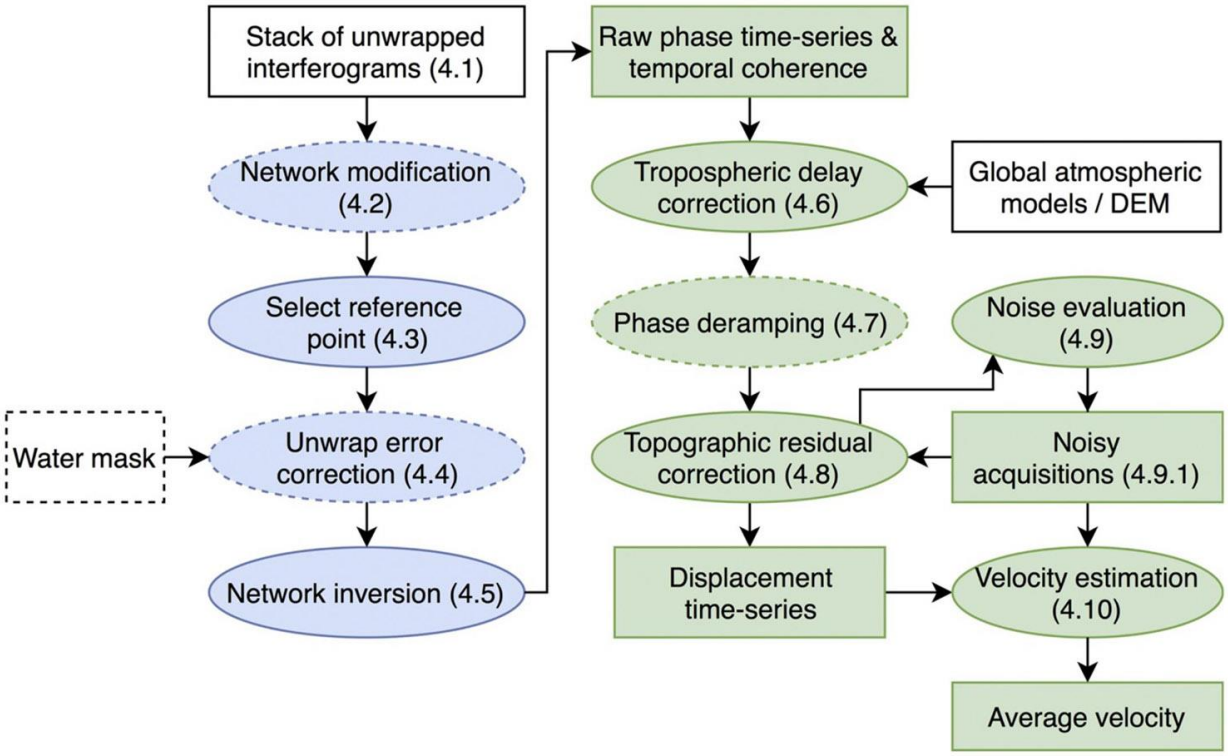

Figure 6 - MintPy SBAS workflow (Zhang et al., 2019).

3. Results and Discussion

The coherence map for the DInSAR analysis can be seen in Figure 7. The coherence history and matrix, and temporal and average spatial coherence for the SBAS analysis can be seen in Figure 8. As expected, the coherence for the DInSAR analysis was low because of the long temporal baseline, and the coherence for the SBAS analysis was much higher because of the time series.

The unwrapped phase to displacement map for the DInSAR analysis can be seen in Figure 9. Generally, displacement maps are filtered by coherence where only displacement values over a certain coherence threshold are displayed. This threshold is typically around 0.6 or 0.7. However, this displacement map was not filtered because the coherence was so low that most of the map would have been filtered out.

The phase to displacement map from the DInSAR analysis (Figure 9) covers a much smaller area than the velocity map from the SBAS analysis (Figure 11, top). A boundary of the study area could not be added during the SBAS analysis using MintPy, but a map showing the study area with the reference point can be seen at the bottom of Figure 11. Because of the vast difference in area analyzed between DInSAR and SBAS, it has difficult to compare the two.

The DInSAR phase to displacement map shows areas of both uplift and subsidence. The transect across the study area (Figure 10) show more subsidence than uplift. The SBAS velocity map also shows areas of uplift and subsidence (Figure 12). The transect across the velocity map approximately crosses the study area, and the subsidence values are similar to that of the DInSAR transect. Overall, the land subsidence was lower than expected, and the uplift was unexpected.

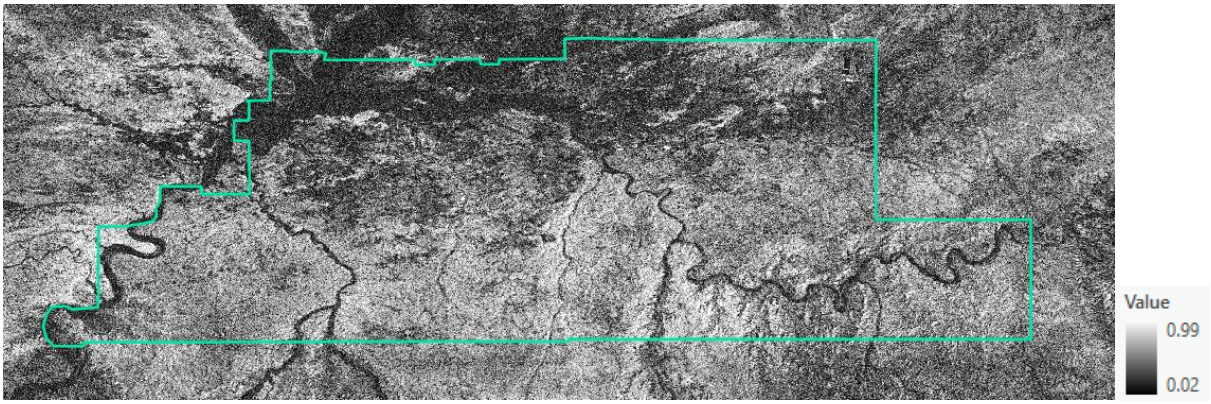

Figure 7 - DInSAR coherence map.

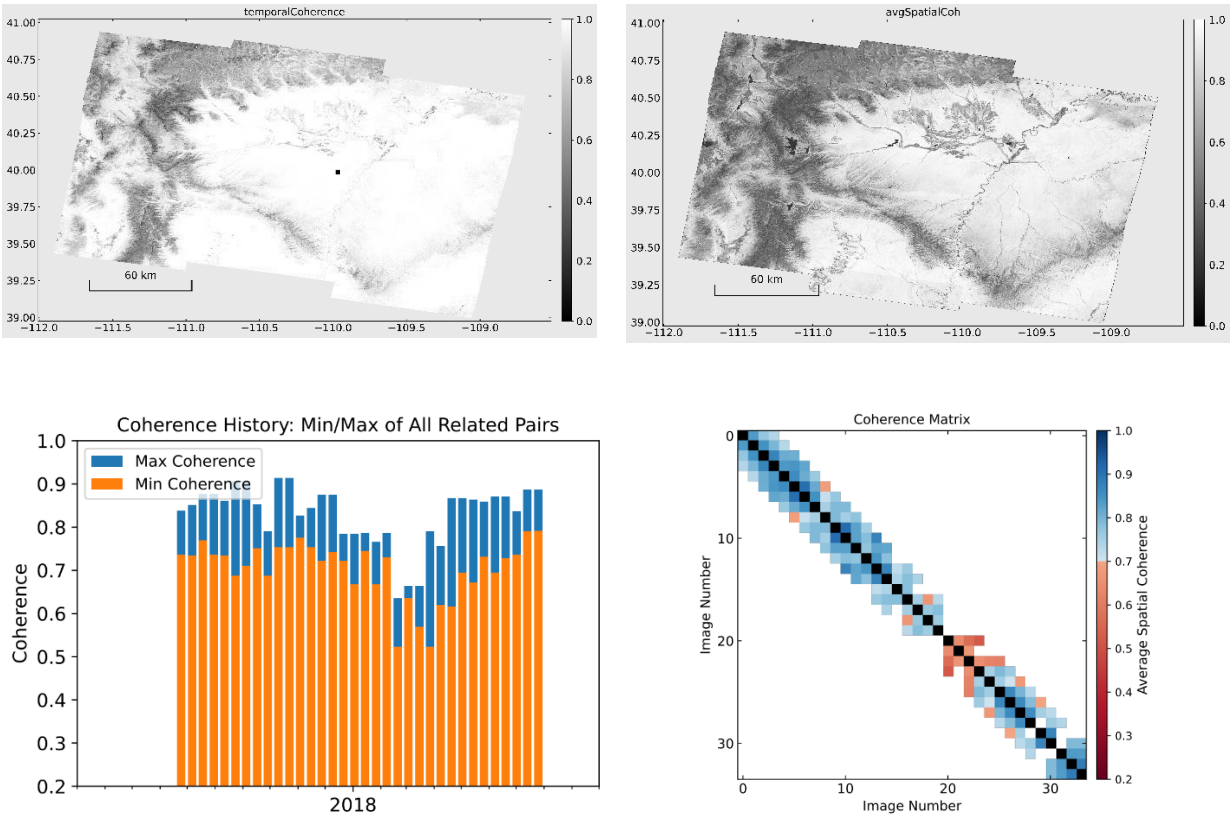

Figure 8 Temporal coherence (top left), average spatial coherence (top right), coherence history (bottom left), and coherence matrix (bottom right) for the SBAS analysis. All graphs and images were generated by MintPy. The square point is the reference point.

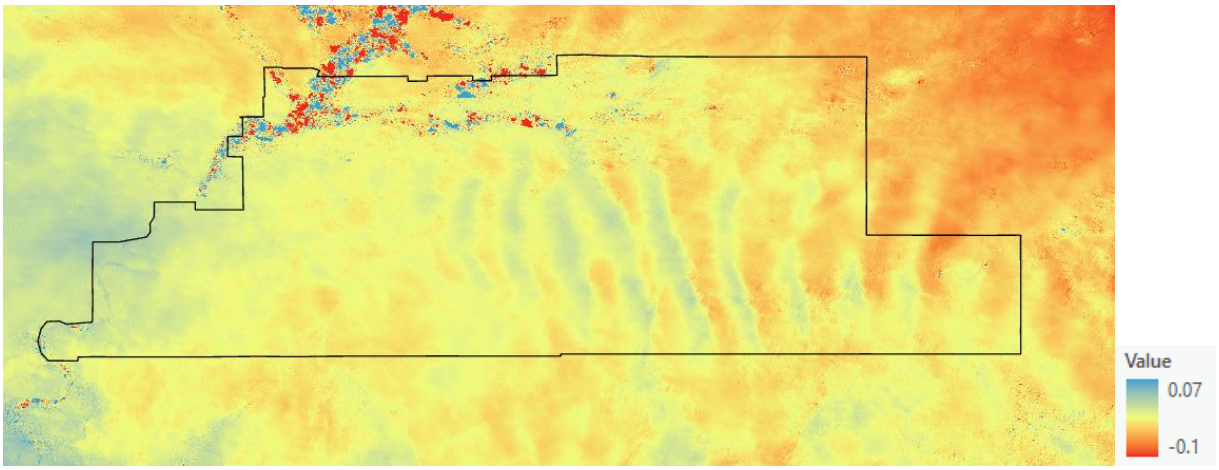

Figure 9 - DInSAR unwrapped phase to displacement map (legend value is meters).

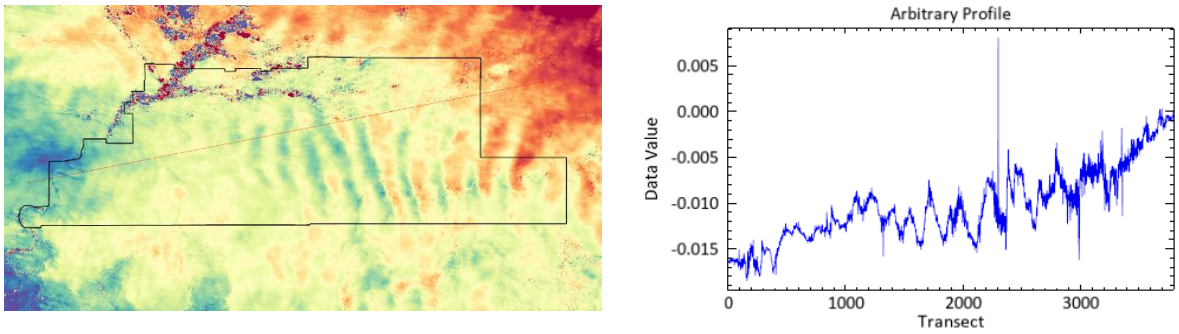

Figure 10 - DInSAR transect of displacement map and values of displacement.

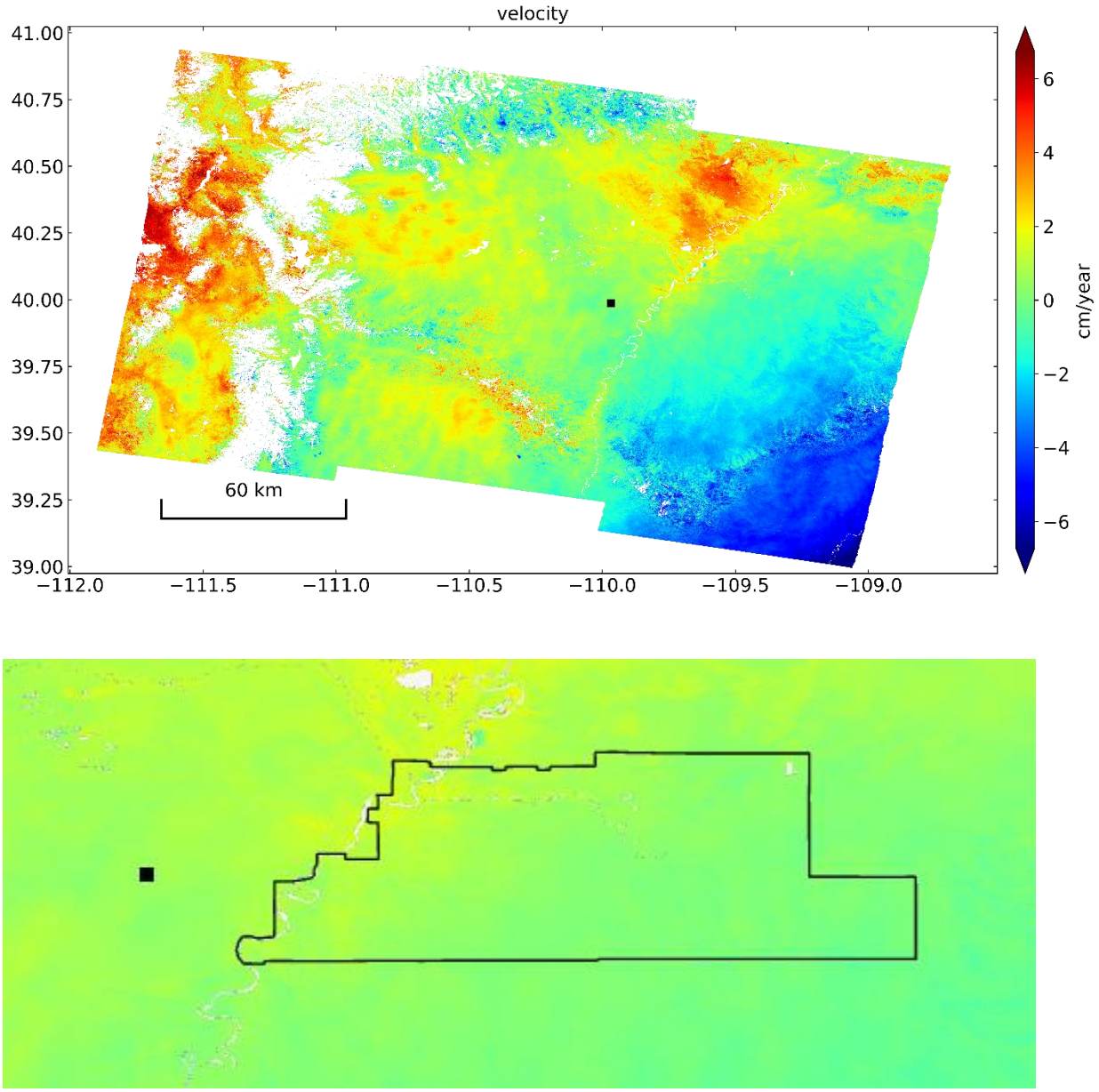

Figure 11 - SBAS analysis velocity map (top). Negative velocities indicate subsidence, and positive velocities indicate uplift. The black square is the reference point. Study area in relation to reference point (bottom).

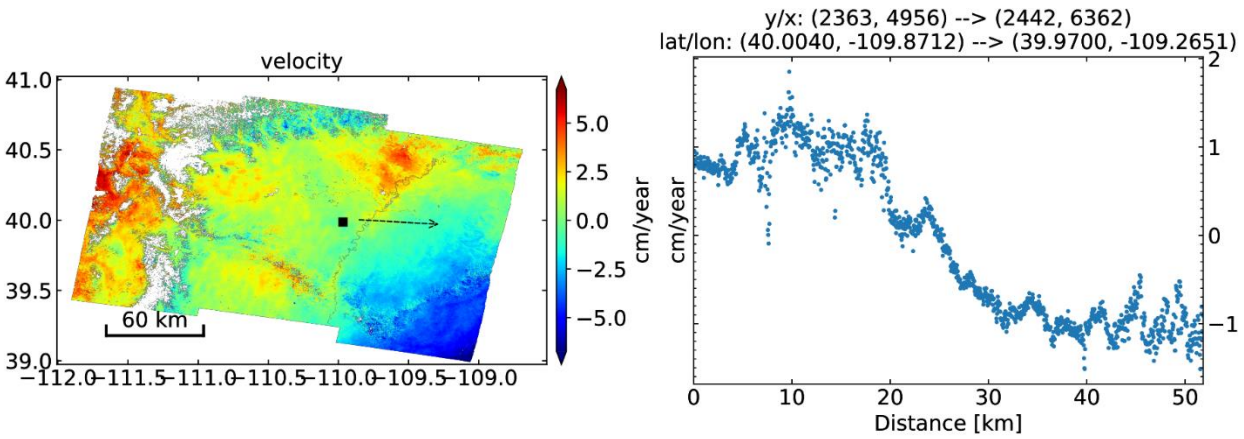

Figure 12 - Transect of velocity map and displacement velocity values along the transect.

The results of the Sentinel-2 imagery classification can be seen in Figure 13, and the accuracy assessment confusion matrix results can be seen in Table 1. An attempt was made to classify agricultural vegetation and natural vegetation separately, but when the classifier could not discern between the two, both classes were merged into one vegetation class. Water in the larger Green River was easily classified, but much of the water in the smaller White River was misclassified as rock; however, the misclassifications were not reflected in the accuracy assessment due to the selection of the ground truth regions of interest.

Table 1 - Accuracy assessment of spectral angle mapper classification in percent.

Class	Desert	Rock	Water	Veg	Total
Desert	100	0	0	0	23.09
Rock	0	100	2.37	0	26.52
Water	0	0	97.63	0	25.84
Veg	0	0	0	100	24.55
Total	100	100	100	100	100

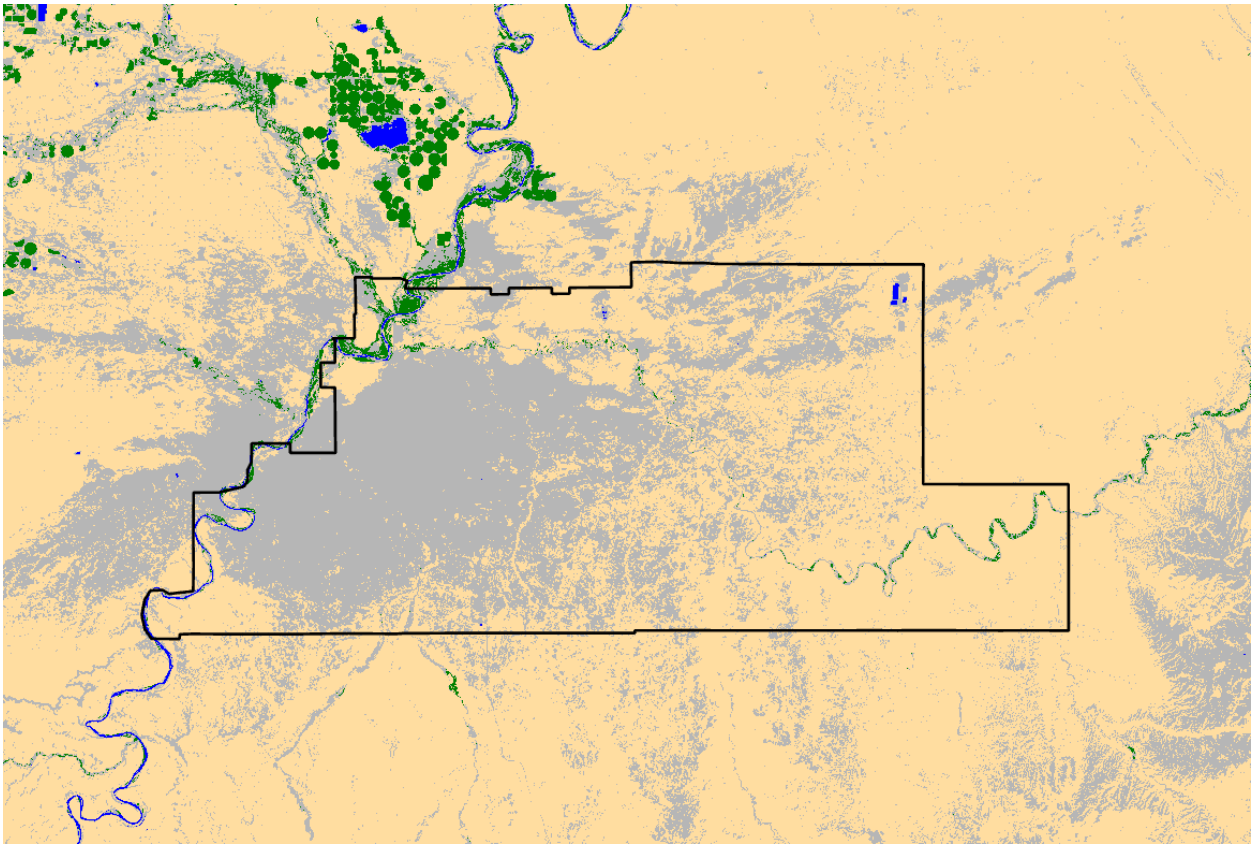

Figure 13 - Spectral angle mapper classification of Natural Buttes study area performed in ENVI. The green is vegetation, blue is water, grey is rock, and yellow is desert.

4. Conclusion

Radar and multispectral remote sensing images are useful for different applications. Radar imagery and InSAR are an excellent choice for detecting land deformation and generating digital elevation models. Multispectral imagery is effective for land classification and detecting landscape changes.

The SBAS analysis proved to be more effective because of the higher coherence between images. A shorter temporal baseline for the DInSAR analysis would have yielded higher coherence; however, it is uncertain if any uplift of subsidence would be detected over a period of

12 to 36 days. In a future study, a PSInSAR analysis could be done along with the SBAS analysis for comparison. Since there are a few structures in the study area, the PSInSAR could be more effective. To improve results of the DInSAR analysis, tropospheric corrections could be made to correct atmospheric errors. In situ GNSS measurements from points in the study area from the beginning and end of the study time frame to determine the accuracy of the analysis results. For a better comparison between the DInSAR and SBAS analysis, it would be better to have the same extent for both analyses.

For the Sentinel-2 classification, a more accurate accuracy assessment could be performed using randomly selected pixels. Additionally, in situ identification of regions of interest could yield more classes and more accurate regions of interest.

References

Alaska Satellite Facility. (n.d.). *Product Guide - HYP3*. Retrieved March 31, 2024, from https://hyp3-docs.asf.alaska.edu/guides/insar_product_guide/#considerations-for-selecting-an-insar-pair

Bagheri-Gavkosh, M., Hosseini, S. M., Ataie-Ashtiani, B., Sohani, Y., Ebrahimian, H., Morovat, F., & Ashrafi, S. (2021). Land subsidence: A global challenge. *Science of the Total Environment, 778*, 146193. https://doi.org/10.1016/j.scitotenv.2021.146193

Chen, X., Tessari, G., Fabris, M., Achilli, V., & Floris, M. (2020). Comparison between PS and SBAS INSAR techniques in monitoring shallow landslides. In *ICL Contribution to Landslide Disaster Risk Reduction* (pp. 155–161). https://doi.org/10.1007/978-3-030-60311-3_17

Chidsey, T. (2022, September 29). Utah's rich oil and gas exploration history. *AAPG EXPLORER*. Retrieved April 7, 2024, from https://explorer.aapg.org/story/articleid/64075/utahs-rich-oil-and-gas-exploration-history

Chidsey, T. C. (2016, July 13). *Energy News: Natural Buttes Field - Utah's "Tight" Sandstone Gas Warehouse - Utah Geological Survey*. Utah Geological Survey. Retrieved April 4, 2024, from https://geology.utah.gov/map-pub/survey-notes/energy-news/energy-news-natural-buttes-field/

Hall, C. (2023, November 21). *What is Synthetic Aperture Radar?* Earthdata. Retrieved March 31, 2024, from https://www.earthdata.nasa.gov/learn/backgrounders/what-is-sar

Karamvasis, K., & Karathanassi, V. (2020). Performance Analysis of Open Source Time Series InSAR Methods for Deformation Monitoring over a Broader Mining Region. *Remote Sensing (Basel)*, *12*(9), 1380. https://doi.org/10.3390/rs12091380

Li, S., Xu, W., & Li, Z. (2022). Review of the SBAS InSAR Time-series algorithms, applications, and challenges. *Geodesy and Geodynamics*, *13*(2), 114–126. https://doi.org/10.1016/j.geog.2021.09.007

Muhammad, H., & Apichontrakul, S. (n.d.). *Vertical Ground Deformation Monitoring of the Sinabung Volcano in 2021- 2022 using Sentinel-1 and DInSAR* [Paper]. 12th International Conference on Environmental Engineering, Science and Management, Pattaya, Thailand. https://www.researchgate.net/publication/370923332

Nozadkhalil, T., Çakır, Z., ErgiNtav, S., Doğan, U., & Walter, T. R. (2023). Land subsidence due to natural gas extraction in the Thrace basin (NW Turkey) and its influence on the North Anatolian fault under the Marmara Sea. *Turkish Journal of Earth Sciences*, *32*(3), 421–430. https://doi.org/10.55730/1300-0985.1852

Suganthi, S., & Elango, L. (2020). Estimation of groundwater abstraction induced land subsidence by SBAS technique. *Journal of Earth System Science*, *129*(1). https://doi.org/10.1007/s12040-019-1298-z

Suhadha, A. G., & Julzarika, A. (2022). Dynamic Displacement using DInSAR of Sentinel-1 in Sunda Strait. *Trends in Sciences (Online)*, *19*(13), 4623. https://doi.org/10.48048/tis.2022.4623

U.S. Energy Information Administration. (2024, March 29). *Natural Gas*. Retrieved April 4, 2024, from https://www.eia.gov/dnav/ng/hist/n9011ut2a.htm

USGS Uinta-Piceance Assessment. (2003). Petroleum systems and geologic assessment of oil and gas in the Uinta-Piceance Province, Utah and Colorado. In *Data series*. https://doi.org/10.3133/ds69b

Zhang, Y., Fattahi, H., & Amelung, F. (2019). Small baseline InSAR time series analysis: Unwrapping error correction and noise reduction. *EarthArXiv (California Digital Library)*. https://doi.org/10.31223/osf.io/9sz6m